Journal of Cerebral Blood Flow & Metabolism (2015) 35, 1313–1322

www.jcbfm.com

ORIGINAL ARTICLE

Imaging the cannabinoid CB1 receptor in humans with [^{11}C]OMAR: assessment of kinetic analysis methods, test–retest reproducibility, and gender differences

Marc D Normandin[1,6], Ming-Qiang Zheng[1], Kuo-Shyan Lin[2], N Scott Mason[3], Shu-Fei Lin[1], Jim Ropchan[1], David Labaree[1], Shannan Henry[1], Wendol A Williams[1], Richard E Carson[1], Alexander Neumeister[4,5] and Yiyun Huang[1]

The Radiotracer [^{11}C]OMAR was developed for positron emission tomography (PET) imaging of cannabinoid type-1 receptors (CB1R). The objectives of the present study were to evaluate kinetic analysis methods, determine test–retest reliability, and assess gender differences in receptor availability. Dynamic PET data were acquired in 10 human subjects, and analyzed with one-tissue (1T) and two-tissue (2T) compartment models and by the Logan and multilinear analysis (MA1) methods to estimate regional volume of distribution (V_T). The 2T model inclusive of a vascular component ($2T_V$) and MA1 were the preferred techniques. Test–retest reliability of V_T was good (mean absolute deviation ~9%; intraclass correlation coefficient ~0.7). Tracer parent fraction in plasma was lower in women ($P < 0.0001$). Cerebral uptake normalized by body weight and injected dose was higher in men by 17% ($P < 0.0001$), but V_T was significantly greater in women by 23% ($P < 0.0001$). These findings show that [^{11}C]OMAR binding can be reliably quantified by the 2T model or MA1 method and demonstrate the utility of this tracer for *in vivo* imaging of CB1R. In addition, results from the present study indicate that gender difference in receptor binding should be taken into consideration when [^{11}C]OMAR is used to quantify CB1R availability in neuropsychiatric disorders.

Journal of Cerebral Blood Flow & Metabolism (2015) **35,** 1313–1322; doi:10.1038/jcbfm.2015.46; published online 1 April 2015

Keywords: cannabinoid CB1 receptor; gender differences; human; kinetic modeling; positron emission tomography; test–retest

INTRODUCTION

The endogenous cannabinoid system consists of two main G protein–coupled receptors: cannabinoid type 1 (CB1), which is located primarily in the brain[1,2] and cannabinoid type 2 (CB2), which is located mainly in immune cells in the periphery.[3] The CB1 receptor has the greatest abundance of seven-transmembrane receptors in the brain with ubiquitous distribution.[4,5] The central cannabinoid system appears to play a modulatory role in the functioning of other neurotransmitter systems and is involved in a wide range of physiologic functions and dysfunctions.[6] Therefore, development of *in vivo* imaging agents for the CB1 receptor will help with the elucidation of its function and potential dysregulation under pathologic conditions.

Efforts to image the CB1 receptor with positron emission tomography (PET) and single-photon emission computed tomography (SPECT) have only recently shown promise.[7] Radioligands that have been successfully advanced to use in human studies include [^{11}C]MePPEP,[8] [^{18}F]FMPEP-d_2,[9] [^{18}F]MK-9470,[10] [^{11}C]SD5024,[11] and [^{11}C]OMAR (also known as [^{11}C]JHU-75528).[12,13]

A recent report investigated the quantification of [^{11}C]OMAR binding in healthy human subjects and patients with schizophrenia.[13] [^{11}C]OMAR was found to exhibit more rapid kinetics—including appreciable washout of radioactivity from most brain regions over the course of the scan duration—and the investigators appropriately chose to use analysis methods that account for reversible binding of the tracer. Logan graphical analysis was used with metabolite-corrected arterial input functions[14] yielding total volume of distribution (V_T, the equilibrium ratio of tracer in tissue relative to plasma) as the primary outcome measure. The authors briefly noted that the Logan plot provided more robust estimates of V_T than did a two-tissue (2T) compartment model, however, a systematic comparison of kinetic analysis methods was not reported.

In the present study, we evaluated [^{11}C]OMAR in a cohort of healthy human subjects. Positron emission tomography data and arterial input functions were acquired and various kinetic analysis methods were compared. Accurate kinetic modeling methods with metabolite-corrected arterial input functions are particularly

[1]PET Center, Department of Diagnostic Radiology, Yale University School of Medicine, New Haven, Connecticut, USA; [2]Molecular Oncology Department, BC Cancer Agency Research Centre, Vancouver, British Columbia, Canada; [3]PET Facility, University of Pittsburgh Medical Center, Pittsburgh, Pennsylvania, USA; [4]Department of Psychiatry, Yale University, New Haven, Connecticut, USA and [5]Molecular Imaging Program, Departments of Psychiatry and Radiology, New York University School of Medicine, New York, New York, USA. Correspondence: Dr YH Huang, PO Box 208048, PET Center, Department of Diagnostic Radiology, Yale University School of Medicine, 801 Howard Avenue, New Haven, CT 06520-8048, USA.
E-mail: henry.huang@yale.edu
This work was supported by NIH RL1 AA017540-03S1, 3RL1 AA017540-03S3, and T32 DA022975. Expert technical assistance was provided by the staff of the Yale Magnetic Resonance Research Center and the Yale PET Center. This research was also made possible by CTSA Grant Number UL1 RR024139 from the National Center for Research Resources (NCRR) and the National Center for Advancing Translational Science (NCATS), components of the National Institutes of Health (NIH), and NIH roadmap for Medical Research. The contents of this publication are solely the responsibility of the authors and do not necessarily represent the official view of NIH.
[6]Present address: Center for Advanced Medical Imaging Sciences, Division of Nuclear Medicine and Molecular Imaging, Department of Radiology, Massachusetts General Hospital, Harvard Medical School, Boston, Massachusetts, USA.
Received 15 October 2014; revised 5 February 2015; accepted 8 February 2015; published online 1 April 2015

important for radiotracer targets where there are no brain regions devoid of receptors that could serve as a suitable reference tissue, as is the case for the CB1 receptor.[4,5,10,13] Modeling outcomes were used to assess the test–retest reproducibility of tracer binding measurements, and to evaluate potential effects of gender on radiotracer metabolism and binding.

MATERIALS AND METHODS

Human Subjects

Ten healthy subjects (five men and five women) of age 18 to 65 years were recruited for this study. Eight of these subjects (four men and four women) underwent test–retest [11C]OMAR studies and two (one man and one woman) underwent single scans. Candidate subjects were screened and confirmed to be free of medical, neurologic, and psychiatric diseases. Additional exclusion criteria included current pregnancy or breastfeeding, history of substance abuse, or positive urine toxicology finding performed on the day of the study. All women underwent PET procedures while in the follicular phase of the estrous cycle. The study protocol was approved by the Yale University Human Investigation Committee, the Yale-New Haven Hospital Radioactive Drug Research Committee, and the Yale University Radiation Safety Committee. Each subject provided written informed consent after the purpose, nature, and potential risks of the studies were explained.

Magnetic Resonance Imaging

A T1-weighted magnetic resonance (MR) image of the brain was acquired for each subject using the MPRAGE pulse sequence on a 3-Tesla scanner (MAGNETOM Trio, Siemens Medical Systems, Erlangen, Germany). Images were reconstructed on a $256 \times 256 \times 176$ grid with $0.98 \times 0.98 \times 1.00$ mm voxels. The subject-specific MR images were used to confirm absence of structural abnormalities in the brain and to provide anatomic localization of PET data in a template space as described below.

Positron Emission Tomography

Radiosynthesis. [11C]OMAR was prepared in high specific activity by previously described procedures[12] adapted for automated production on the GE TRACERlab FXC-Pro synthesis module (GE Healthcare, Milwaukee, WI, USA). Radiochemical purity was $>90\%$. Radioactivity dose was 676 ± 65 MBq and injected mass dose was 29 ± 11 ng/kg ($n = 18$).

Imaging. Positron emission tomography scanning was performed on the high-resolution research tomograph (HRRT) camera (Siemens Medical Systems, Knoxville, TN, USA). Retest scans were performed the same day with radiotracer injections separated by ~3.5 hours. For each session, the subject was positioned in the bore of the camera and a transmission scan was performed using a ^{137}Cs point source. [11C]OMAR was administered via the antecubital vein as a slow bolus over 60 seconds with an automated syringe pump (PHD2000, Harvard Apparatus, Holliston, MA, USA). Emission data were obtained in listmode for 120 minutes. Subject motion was monitored using an optical system (Polaris Vicra, Northern Digital Incorporated, Waterloo, Ontario, Canada) positioned behind the PET scanner, which at 50 ms intervals recorded the three-dimensional position and orientation of the infrared reflective tool mounted rigidly to the subject's head using a Lycra cap and Coban self-adherent wrap. The optical tracking data were synchronized to the listmode emission measurements and used in the motion-compensation OSEM algorithm[15] to generate PET images corrected for subject motion, event by event, as well as photon scatter and attenuation, random coincidences, system deadtime, and detector inhomogeneity. The dynamic image sequences had 33 frames with increasing duration: 6×30 seconds, 3×1 minutes, 2×2 minutes, and 22×5 minutes.

Arterial blood measurements. Arterial blood was sampled from the radial artery to determine the radiotracer input function. Prior to tracer injection, a 6-mL sample was drawn and ~6 MBq of [11C]OMAR solution was added. Free fraction of the tracer in plasma (f_p) was determined in triplicate from this sample by the ultracentrifugation method. Radioactivity concentration in arterial whole blood was measured continuously during the first 7 minutes after [11C]OMAR administration using an integrated peristaltic pump and radioactivity detection system (PBS101, Veenstra Instruments, Joure, The Netherlands). Afterward, discrete samples were manually drawn at 3, 5, 7, 10, 15, 20, 30, 45, 60, 75, 90, 105, and 120 minutes after injection. The whole blood and plasma radioactivity in each manual sample was measured using a gamma counter (Wizard 1480, PerkinElmer, Waltham, MA, USA) and converted to concentration according to the weight and density of the measured aliquot. The ratio of radioactivity in plasma and whole blood was determined from the discrete samples and used to scale the whole blood concentration measured by the continuous counter in the first few minutes after tracer administration. Samples acquired at 5, 15, 30, 60, and 90 minutes were analyzed by the column-switching high-performance liquid chromatography (HPLC) method[16] to determine the fraction of unmetabolized radiotracer. Plasma samples were treated with urea (8 mol/L) and citric acid (50 mmol/L) to eliminate plasma protein binding, passed though a 0.45-μm syringe filter (Millex-HA, EMD Millipore, Darmstadt, Germany), and loaded onto a capture column (19×4.6 mm) packed with C18 sorbent (Strata-X SPE, Phenomenex, Torrance, CA, USA) eluting with 1% acetonitrile in water at 2 mL/min. The trapped activity was then eluted onto a Phenomenex Synergi Polar-RP HPLC column (250×4.6 mm, 5 μm) with a mobile phase of 65% acetonitrile and 35% 50 mmol/L ammonium acetate adjusted to pH 5.8 with acetic acid. High-performance liquid chromatography eluent was collected in an automated fraction collector (Spectra/Chrom CF-1, Spectrum Chromatography, Houston, TX, USA). Radioactivity in the filtered plasma–urea mixture, filters, and HPLC fractions were measured using the gamma counter. The sample recovery rate, extraction efficiency, and HPLC fraction recovery rate were determined for each sample. The unmetabolized parent fraction was calculated as the ratio of the sum of radioactivity in fractions containing the parent compound to the total amount of radioactivity collected, and fitted with an inverted gamma function. The parent fraction curve was also normalized by the time-varying extraction efficiency of radioactivity for the corresponding filtered plasma sample. The final metabolite-corrected arterial plasma input function was calculated as the point-by-point product of the total plasma radioactivity concentration curve and the parent fraction curve.

Image analysis. Positron emission tomography images summed from 0 to 10 minutes after injection were rigidly aligned using Affine Inter-modal Image Registration (FLIRT)[17] to the subject-specific MR image, which was in turn warped using a nonrigid registration routine[18] to a standard MR template where regions of interest (ROIs) were delineated according to the Anatomical Automatic Labeling (AAL) atlas.[19] Regional time–activity curves (TACs) were analyzed using compartmental models and graphical techniques with metabolite-corrected arterial input functions. The primary outcome measure was the total volume of distribution (V_T), which reflects the equilibrium ratio of radiotracer concentration in tissue relative to arterial plasma.[20] One-tisse or two-tissue compartment models were assessed without (1T, 2T) or with ($1T_V$, $2T_V$) explicit contribution of radioactivity from the vascular fraction of the tissue using the measured whole-blood TAC, and with the blood volume included as an estimated parameter. The Logan graphical analysis[14] and multilinear analysis (MA1)[21] methods were applied with cutoff time t^* ranging from 0 to 60 minutes in 10-minute increments.

Variability and reproducibility assessment. Within-subject changes in V_T between imaging sessions were calculated according to the formula $\Delta V_T = 2^*(V_{T1} - V_{T2})/(V_{T1}+V_{T2})$, with the numeric subscripts distinguishing values from scans 1 (test) and 2 (retest). The average ΔV_T across subjects was determined for each ROI to measure any systematic changes between scans and the standard deviation (s.d.) was calculated as an index of variability. The mean absolute deviation, $2^*|V_{T1} - V_{T2}|/(V_{T1}+V_{T2})$, a frequently reported metric of reliability, was also tabulated. Finally, the intraclass correlation coefficient (ICC), which expresses within-subject variability in relation to between-subject variability, was calculated for the regional V_T estimates. A Bland–Altman difference plot was generated to compare regional V_T estimates between the first and second scans for each subject.

Sex differences. Plasma protein binding, plasma metabolite fraction, net brain uptake (Standard Uptake Value, SUV), and V_T were compared between men and women to assess the effect of sex on these parameters. To avoid undue emphasis of certain subjects caused by repeated measures and to mitigate the possibility that the scan order could have systematic effects (e.g., because of circadian oscillations or differential anxiety levels between the first and second scans), group-wise comparisons between men and women were performed with data from the retest scans omitted.

Statistical Analysis

Quantitative results are presented as mean ± s.d. unless otherwise noted. Differences between groups were assessed using a two-tailed Student's *t*-test with heteroscedastic variance. Two-way analyses of variance were performed to compare [11C]OMAR uptake across gender and regions, and to compare blood measurements across gender and time after injection. *Post hoc* testing of individual regions and time points was performed with Bonferroni correction for multiple comparisons. The level of significance was defined as $\alpha = 0.05$ for all tests, which were conducted using GraphPad Prism 6 (GraphPad Software, La Jolla, CA, USA).

RESULTS

Arterial Plasma Measurements

Arterial plasma analysis showed a moderate rate of radiotracer metabolism, with 51% ± 8% and 30% ± 6% of unmetabolized [11C]OMAR at 30 and 90 minutes after injection, respectively (Figure 1). All radiometabolites eluted from the HPLC column earlier than [11C]OMAR, suggesting that they are more polar and not likely to penetrate the blood–brain barrier. The f_p value measured by ultrafiltration was very low at 0.0022 ± 0.0008 across scans. After the peak, metabolite-corrected plasma concentrations were described well by a biexponential function with half-lives of 6.3 ± 1.8 and 74 ± 20 minutes, with the slow component contributing 75% ± 7% of the integral of the curve extrapolated to infinity. Total plasma clearance was calculated to be 636 ± 189 mL/kg/h.

Uptake of [11C]OMAR and Time–Activity Curves (TACs) in the Brain

High uptake of [11C]OMAR was observed in the lentiform nucleus (pallidum and putamen), anterior cingulate gyrus, insula, cortical subregions, and cerebellar cortex; lower uptake was in white matter and diencephalon. These qualitative uptake patterns, as shown in the representative PET and coregistered MR images in Figure 2, are in very good agreement with previous imaging studies using other CB1 radiotracers.[8–10,13]

After an initial peak attributable to high concentration of tracer in the vasculature relative to tissue, [11C]OMAR concentrations in most brain regions reached a maximum at 20 to 25 minutes after injection with SUV ranging from 0.5 to 1.4. Kinetics of TACs was similar to that previously observed in nonhuman primates[12] with cerebral clearance generally faster than other CB1 ligands reported in humans.[8–10] Regional TACs averaged across scans are portrayed in Figure 3.

Assessment of Modeling Methods

Time–activity curves from most regions were fitted poorly by a 1T compartment model, with or without inclusion of a vascular component (1T and $1T_V$). The 2T model without a blood contribution V_T values generally provided visually reasonable fits, however, addition of the blood volume fraction to the model (2Tv) was considered statistically justified by the Akaike and Bayesian information criteria.[22,23] Of the 306 regional TACs analyzed (18 scans by 17 ROIs), the $2T_V$ model failed to converge to physiologically plausible parameter values (see Discussion section) for three data sets, one in the amygdala and two in the hypothalamus; hence those data are excluded from subsequently reported findings. The blood volume fractions estimated by $2T_V$ were physiologically reasonable but quite variable, averaging 3.5% ± 1.9% (coefficient of variation = 54%) across all data sets, and yielded V_T estimates that were 1.7% ± 2.6% lower than the 2T values, but correlated strongly with 2T values without a vascular component ($y = 1.03x+0.01$, $R^2 = 0.99$; Figure 4C). Although the 1T model fits were typically not satisfactory as noted above, the estimated V_T values were generally in good agreement with those obtained using the $2T_V$ model ($y = 0.90x - 0.05$, $R^2 = 0.94$ for $1T_V$; $y = 0.95x - 0.04$, $R^2 = 0.95$ for 1T; see Figures 4A and 4B). The Logan and MA1 graphical methods both provided good fits to the transformed data when t^* was set to at least 20 or 30 minutes, depending on the brain region. Volume of distribution values obtained with MA1 showed slightly stronger correlation with those estimated using the $2T_V$ model, but V_T values derived from both graphical methods were in excellent agreement with those from the $2T_V$ model ($y = 1.02x+0.00$, $R^2 = 0.97$ for MA1; $1.00x+0.01$, $R^2 = 0.95$ for Logan graphical analysis; see Figures 4D and 4E). The V_T values estimated by the $2T_V$ model showed regional heterogeneity ranging from 0.9 mL/cm^3 in central white matter to 1.6 mL/cm^3 in the pallidum (Figure 5A). Intersubject variability in V_T was 15% to 20% coefficient of variation. K_1 values were low, consistent with the very low f_p, averaging 0.04 to 0.05 mL/min/cm^3 in most regions (Figure 5B).

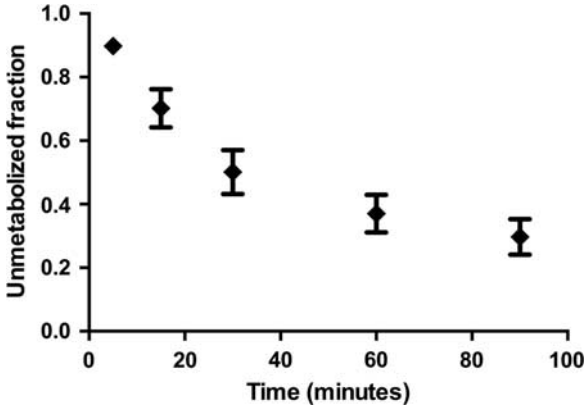

Figure 1. Parent fraction of [11C]OMAR in the plasma. Data points represent the mean across all scans. Error bars show the s.d.

Test–Retest Variability and Reproducibility

Variability of [11C]OMAR V_T estimates between scan sessions was relatively low. Across subjects, mean ΔV_T was ~2% using the $2T_V$ model and 1% using MA1, with s.d. ⩽ 12% in most regions for either method. For MA1, intraclass correlation coefficient ranged from 0.51 (parietal cortex) to 0.85 (posterior cingulate cortex), with typical values of ~0.7 (Table 1). Intraclass correlation coefficient with the $2T_V$ model indicated slightly worse reliability, with typical values of 0.65. Within a given subject, all ΔV_T values were typically positive or negative across regions, suggesting that measurement error in the input function may be a primary source of variability. Otherwise, there was no systematic effect of scan order. The Bland–Altman difference plot depicted in Figure 6A reiterates the reproducibility of regional V_T estimates obtained with MA1, showing low bias (average absolute difference of 0.011), good precision (s.d. of 0.132 for absolute differences), and lack of any obvious relationship between the magnitude of the parameter and its corresponding bias or variability. Of the 136 regional V_T pairs (17 ROIs by eight test–retest subjects), 7 were outside the 95% confidence interval; notably, all were from the same subject. Application of linear regression for the Bland–Altman differences further underscored the general findings, with the fit yielding a small slope (−0.048 ± 0.045; $R^2 = 0.008$ and $P = 0.29$ for nonzero slope) and intercept (0.070 ± 0.055). The high quality of the fit (75 zero crossings and $P = 0.93$ for deviation from linearity by the runs test) is evident from the residuals plot, which again reveals no systematic dependence of bias or variance on the magnitude of V_T (Figure 6B).

Gender Differences

Men and women participating in this study did not differ in age (32 ± 8 versus 26 ± 6 years; $P = 0.23$), injected activity (655 ± 63 versus 693 ± 54 MBq; $P = 0.33$), injected mass (2.2 ± 0.4 versus 2.1 ± 0.9 μg; $P = 0.74$), injected mass dose normalized by body

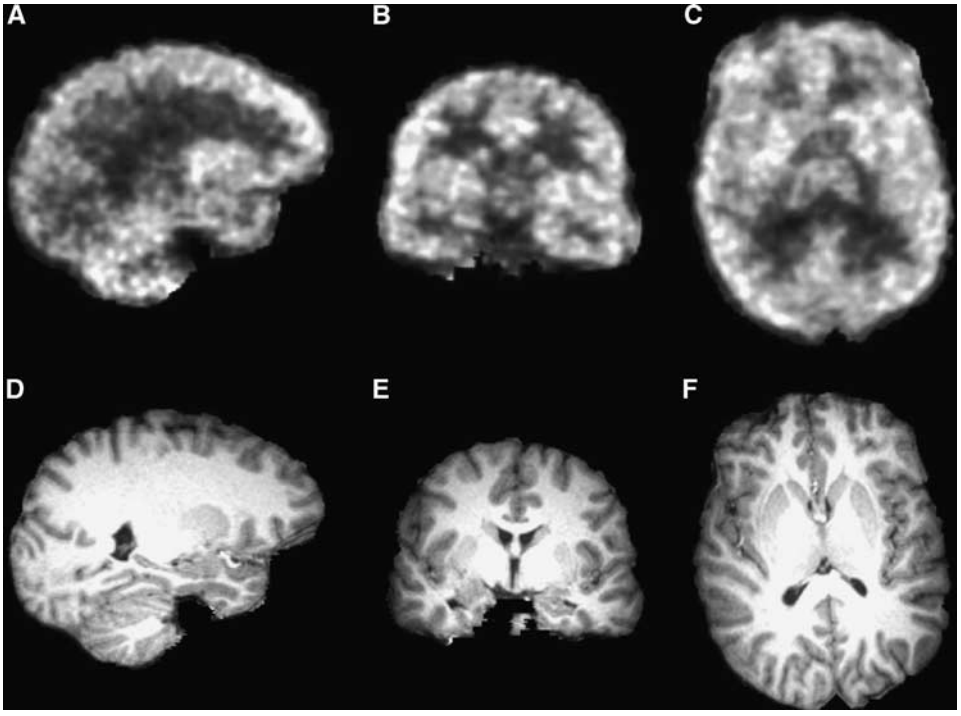

Figure 2. Representative positron emission tomography (PET) images summed 40 to 60 minutes after injection of 680 MBq of [11C]OMAR (**A**–**C**) and subject's T1-weighted magnetic resonance (MR) images (**D**–**F**) shown in the same space as reconstructed PET data. Sagittal slices shown in **A** and **D**, coronal slices in **B** and **E**, and axial slices in **C** and **F**.

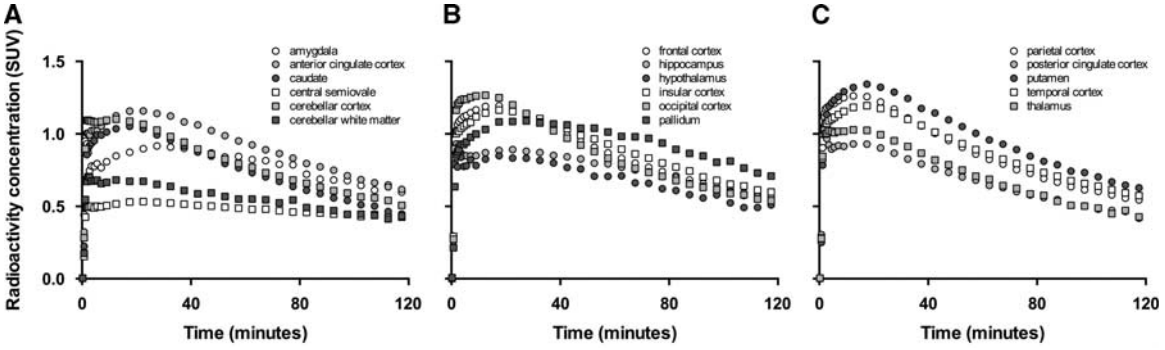

Figure 3. Regional time–activity curves averaged across all subjects. Separate panels (**A**, **B**, and **C**) shown only to aid visibility. Regional uptake of [11C]OMAR was in fairly good agreement with the known density and distribution of cannabinoid type 1 (CB1) receptors in the brain (see Supplementary Figure 1).

weight (29 ± 5 versus 36 ± 15 ng/kg; $P = 0.44$), or level of education (16 ± 3 versus 16 ± 2 years; $P = 0.68$). Although men were heavier by raw body weight (77 ± 9 versus 59 ± 6 kg; $P = 0.009$), there were no significant group differences in body mass index (26 ± 3 versus 23 ± 2 kg/m^2; $P = 0.11$).

Tracer free fraction in plasma did not differ between sexes (0.0022 ± 0.0008 in men, 0.0022 ± 0.0012 in women; $P = 0.98$; Figure 7A), however, the average parent fraction in the plasma was higher in men (e.g., 0.65 ± 0.09 at 30 minutes versus 0.53 ± 0.08 in women) at all measured time points (Figure 7B). The two-way analysis of variance on plasma radiometabolite fraction revealed that the effect of gender was statistically significant ($P < 0.0001$ for global effect; differences at 15 and 30 minutes after injection survived multiple comparisons correction), but the interaction between sex and time after injection was not ($P = 0.78$). Gender differences in whole blood and plasma total radioactivity concentrations normalized by injected dose and body weight (i.e., SUV) were significant (greater in men than women, $P < 0.0001$ for global effects; see Figures 7C and 7D), as were the interactions between gender and time ($P < 0.0001$) reflecting the substantial differences primarily during the initial distribution phase (for both whole blood and plasma radioactivity concentrations, group differences survived multiple comparisons correction for the 3- and 5-minute time points whereas all other time points were strongly nonsignificant with $P > 0.99$). Integrated brain TACs from men had greater numerical mean SUV across all but one region (Figure 7E) with values 17% higher on average ($P < 0.0001$ for effect of sex, no interaction between sex and region; no individual regions survived Bonferroni correction), consistent with previous findings obtained using the CB1 PET tracer [18F]MK-9470.[24] Mean values of V_T, however, were higher in women across the 17 ROIs examined (Figure 7F) with an average

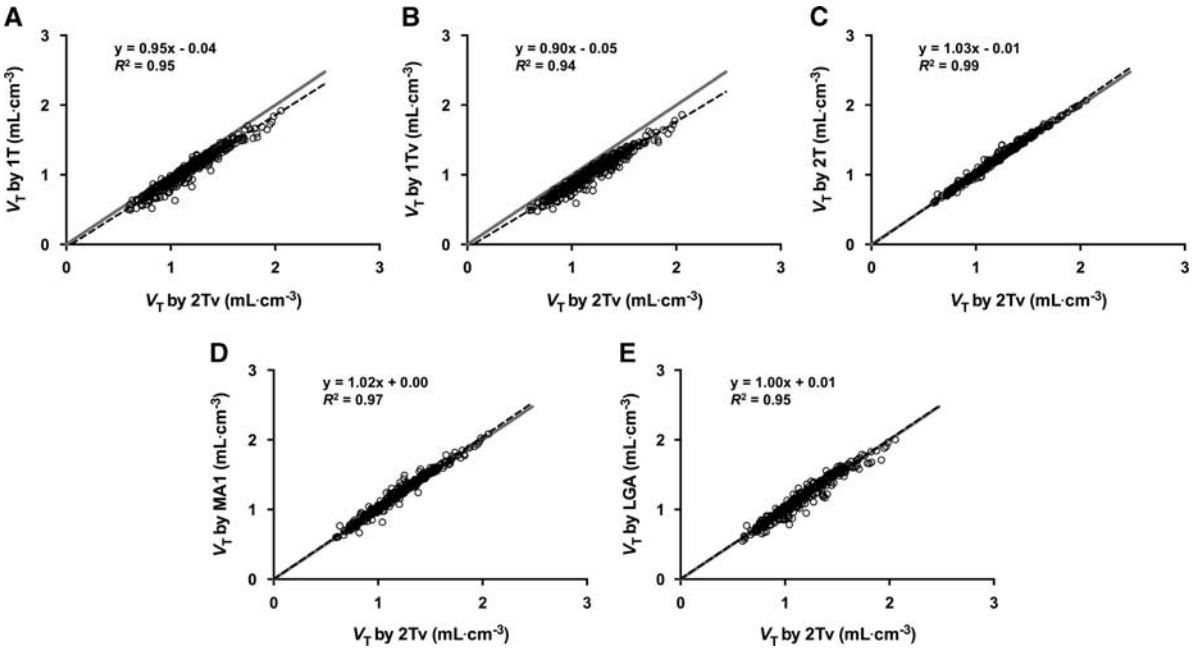

Figure 4. Correlation of volume of distribution (V_T) values estimated by alternative analysis methods against those obtained using the preferred compartmental model, $2T_V$. Dashed black lines show the linear regression line with the regression equation and correlation coefficient indicated on each panel. Solid gray lines designate the line of identity. Each marker represents the values estimated for a given region for a particular scan, with display of results from the 17 brain regions in each of 18 positron emission tomography (PET) scans.

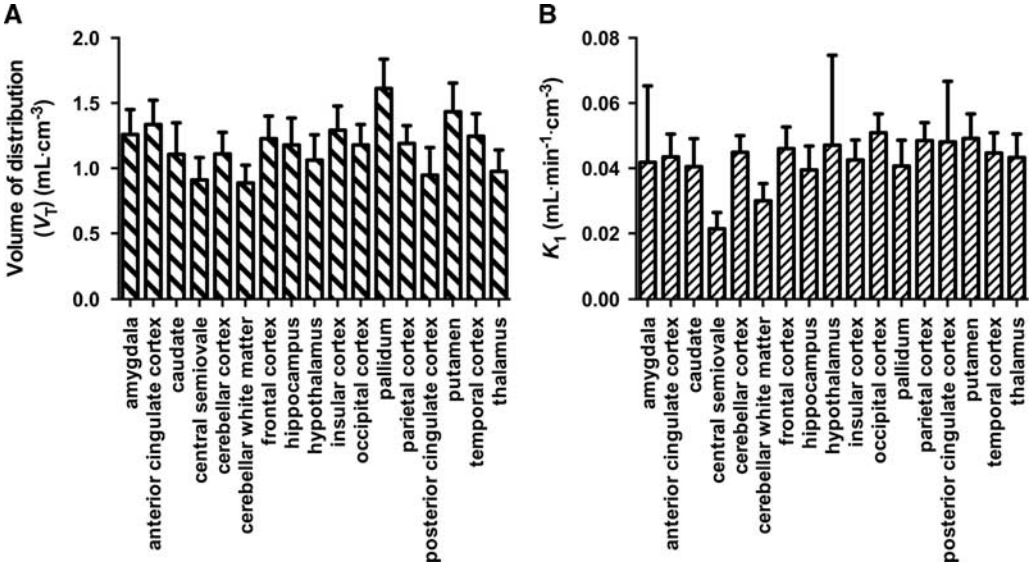

Figure 5. Values of V_T, (**A**) and K_1 (**B**) estimated by the $2T_V$ model. Data show the average across all subjects with error bars indicating 1 s.d. Intersubject variability in V_T was typically 15% to 20%.

difference of 23% ($P < 0.0001$ for effect of gender, no interaction between gender and region in analysis of variance; *post hoc* testing revealed differences that survived multiple comparison testing in caudate, pallidum, posterior cingulate cortex, and putamen with frontal cortex, hippocampus, and temporal cortex also contributing to global effect with $0.05 <$ adjusted $P < 0.10$).

DISCUSSION

We present findings from a PET study evaluating the radiotracer [11C]OMAR for imaging CB1 receptor in healthy human subjects. The data acquired in these experiments were used to assess quantification methods, investigate reproducibility of measurements, and explore differences in pharmacokinetics and binding parameters between men and women. Here we provide commentary on our findings as they relate to the overall appraisal and utility of [11C]OMAR.

Several kinetic analysis methods were applied to determine the optimal methods for quantification of [11C]OMAR images. As the CB1 receptor is distributed ubiquitously throughout the brain[4,5] and a suitable reference tissue devoid of specific tracer binding has not been identified for [11C]OMAR or other CB1 radioligands,[10,11] all analyses used metabolite-corrected arterial input functions. Among the compartmental methods, the 1T model

provided inadequate fits to the data whether the model equations included correction for radioactivity in the vasculature ($1T_V$ model) or not (1T). Although the 2T model generally provided visually satisfying fits without correcting for the blood signal (2T), the Akaike and Bayesian information criteria deemed inclusion of the vascular term ($2T_V$) to be statistically justified in the majority of cases. This is attributable to the poor first pass extraction of [^{11}C]OMAR—potentially mediated by high plasma protein binding—as indicated by the low K_1 values (~0.05 mL/min/cm^3; Figure 5B), resulting in relatively low concentration of radioactivity in tissue relative to blood at early time points. The $2T_V$ model was thus considered the preferred compartmental analysis method.

Despite the fact that the 1T models fit the data poorly, they still provided V_T values in reasonable agreement with the 2T model results (Figures 4A and 4B). The Logan (LGA) and MA1 graphical analysis methods were also assessed. Whereas in preclinical studies, we found the Logan method to suffer heavily from its familiar susceptibility to noise-induced bias,[25] in these clinical studies, we observed scant evidence of such an effect as indicated by slight underestimation of LGA V_T relative to 2T results (Figure 4E); such effects may still be present in voxelwise analyses using Logan graphical method. MA1 V_T values were in even better agreement with compartmental modeling results, both in terms of further minimization of bias as well as strength of correlation, and is therefore endorsed as the linear method of choice for [^{11}C]OMAR imaging data analysis. MA1 proved to be somewhat more robust than $2T_V$, as exemplified by higher ICC and lack of physiologically unreasonable V_T estimates. In addition to improved reliability, it is noted that MA1 is computationally more efficient to apply than the 2T models. Based on these considerations, MA1 has been adopted for use in our clinical research studies[26,27] and is the recommended analysis method unless knowledge of the compartmental model's microparameters (e.g., K_1, k_2, k_3, and k_4 for the 2T model) is required in addition to the macroparameter V_T, the primary binding outcome measure for reversible radioligands in the absence of a reference tissue.

Table 1. Metrics of test–retest reproducibility for [^{11}C]OMAR V_T values estimated by MA1

Region	*Mean ΔV_T (%)*	*s.d. ΔV_T (%)*	*m.a.d. ΔV_T (%)*	*ICC*
Amygdala	1.5	12.0	8.4	0.79
Anterior cingulate cortex	0.2	11.3	7.8	0.68
Caudate	−0.2	13.5	9.8	0.79
Central semiovale	2.3	14.1	9.9	0.71
Cerebellar cortex	0.6	13.1	10.0	0.59
Cerebellar white matter	3.2	11.8	9.2	0.54
Frontal cortex	0.4	11.6	8.1	0.67
Hippocampus	2.4	12.5	8.9	0.72
Hypothalamus	3.7	12.0	9.9	0.72
Insular cortex	0.2	11.9	8.4	0.63
Occipital cortex	0.8	11.0	7.6	0.65
Pallidum	1.2	12.1	7.9	0.63
Parietal cortex	1.0	11.7	8.8	0.51
Posterior cingulate cortex	1.5	11.2	8.8	0.85
Putamen	0.1	10.4	7.3	0.74
Temporal cortex	0.5	10.9	7.9	0.70
Thalamus	1.2	11.6	7.6	0.75
Median	1.0	11.8	8.4	0.70
Mean	1.2	11.9	8.6	0.69

Abbreviations: ICC, intraclass correlation coefficient; MA1, multilinear analysis; m.a.d., mean absolute deviation; V_T, volume of distribution.

In our test–retest studies, we observed that although there was no systematic effect of scan order across subjects (Table 1), for a given subject the regional V_T values tended to all increase or decrease from one scan to the next. This could not be attributed to carryover mass between injections, which would preferentially depress V_T in the second scan. Nor is it likely that diurnal effects caused these intrasubject changes, because the timing of the first and second scans was consistent at ~09:30 and 13:00, respectively, for all subjects. Rather, we interpret these results as an indication that measurement error in the arterial input function, common to the analysis of all brain regions, may be a primary source of variability. Indeed, it has previously been noted that the improved performance of [^{18}F]FMPEP-d_2 over [^{11}C]MePPEP is attributable in large part to more reliable measurement of the blood data.[9] Hence, it may be possible to further improve the quantitative reliability of [^{11}C]OMAR through refinement of the arterial input function measurements.

[^{11}C]OMAR was developed by Horti and colleagues[13] and has been used in a clinical investigation of the CB1 receptor in schizophrenia. In that study, the subjects were almost exclusively men ($n = 10$ control subjects, all men; $n = 6$ schizophrenic subjects, one woman). Regional TACs were plotted for the control subjects as were the corresponding V_T values estimated using Logan graphical analysis with an arterial input function, with both showing high correspondence with the measurements made in the present study (Figures 3 and 5A). Similarly, the average parent ligand in plasma was 41% at 60 minutes in their predominantly

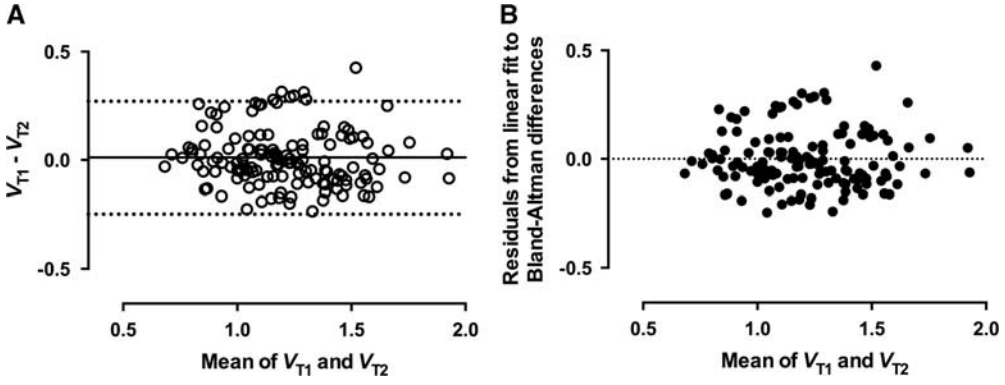

Figure 6. (**A**) Bland–Altman plot showing the difference in regional volume of distribution (V_T) values between test and retest scan sessions versus the mean of the estimated values. Solid horizontal line represents the bias (0.011), while the dashed lines depict the 95% confidence interval (−0.248 to 0.271). (**B**) Residuals from linear regression applied to the data in the Bland–Altman plot. The linear fit was of high quality and the resulting regression equation had a small slope and intercept (see text for details), reiterating the lack of discernible pattern in the Bland–Altman difference plot. Dashed horizontal line represents $y = 0$.

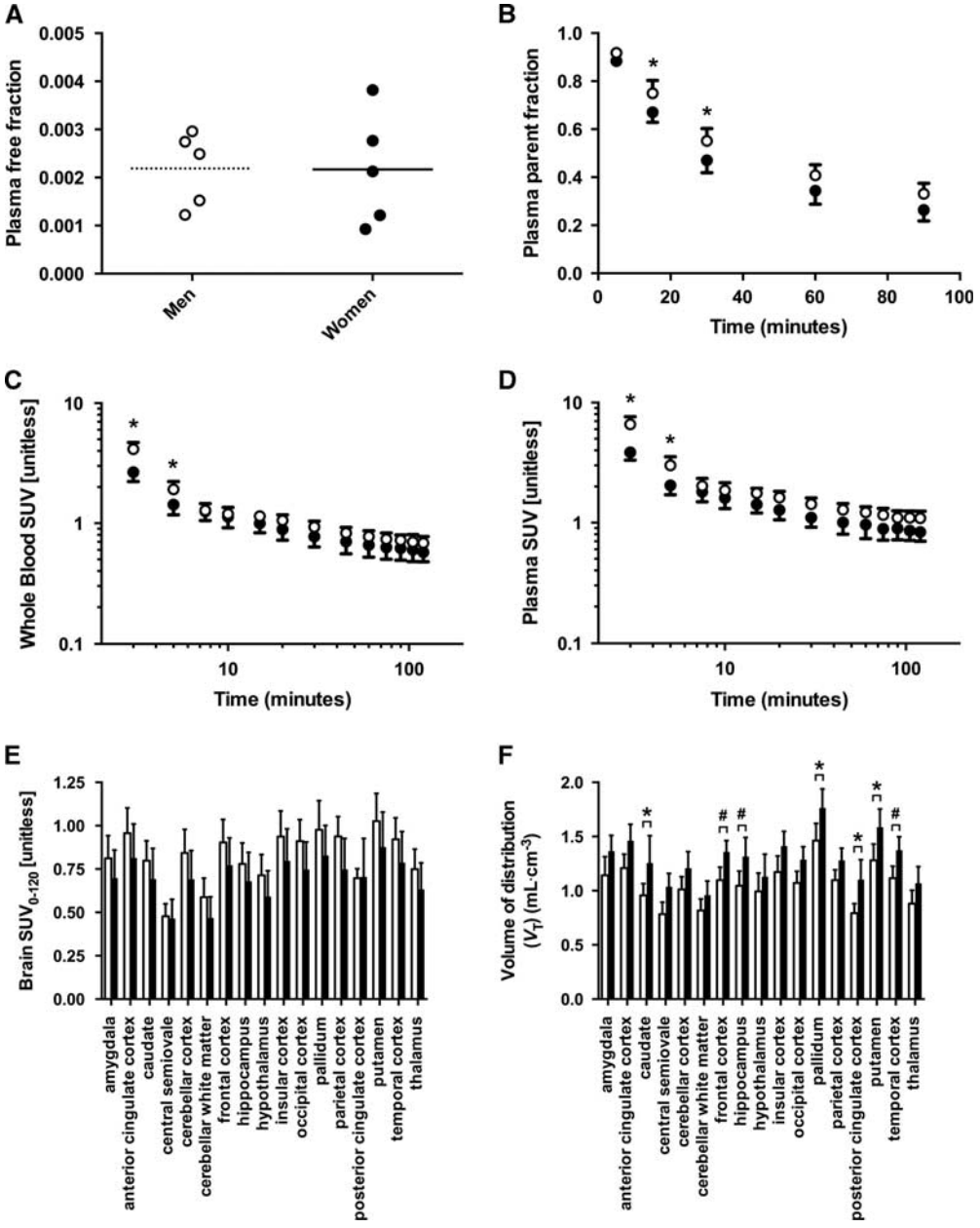

Figure 7. Comparison of [11C]OMAR blood and brain data between genders. (**A**) Plasma protein binding did not differ between sexes ($P = 0.78$). (**B**) Fraction of radioactivity in the plasma attributable to the parent compound was greater in men than women ($P < 0.0001$ for global effect of gender). (**C**) Whole blood and (**D**) total plasma radioactivity concentrations were greater in men ($P < 0.0001$ for global effect as well as for interaction between sex and time). (**E**) Net brain uptake of [11C]OMAR, as reflected by SUV over the 0 to 120-minute window, was ~17% greater in men across brain regions ($P < 0.0001$ for effect of sex). (**F**) Regional V_T values estimated by multilinear analysis (MA1) were ~23% greater in women than men ($P < 0.0001$). Data from men are depicted by open markers/bars and data from women by filled markers/bars. *$P < 0.05$ and #$0.05 \leqslant P < 0.1$, adjusted P values after Bonferroni correction for multiple comparisons.

male cohort, which is in excellent agreement with our findings in the present study (parent fraction of 0.41 ± 0.04 in men at 60 minutes; Figure 7B). It is further noted that these two studies shared several methodological commonalities, including use of the HRRT scanner and column-switching HPLC for radiometabolite analysis, and we conclude that the results obtained are highly concordant between the two sites.

In addition to [11C]OMAR, other CB1 radiotracers that have recently been used in humans include [18F]MK-9470, [11C]MePPEP, [18F]FMPEP-d_2, and [11C]SD5024. These PET tracers are structurally related to the CB1 inverse agonist rimonabant (SR141716) or taranabant and have high lipophilicity.[7,11] [11C]OMAR exhibits brain uptake similar to that of [18F]MK-9470 (peak SUV ~ 1.4),[10,28] but less than that of [11C]SD5024 (peak SUV ~ 2.5),[11] [11C]MePPEP (peak SUV ~ 4)[8] and [18F]FMPEP-d_2 (peak SUV ~ 5).[9] [11C]OMAR has relatively modest CB1 affinity, with $K_i = 11$ nmol/L, or 2.1 nmol/L, in contrast to other radiotracers that exhibit subnanomolar affinities.[7,11] This relatively lower affinity imparts faster pharmacokinetics. The slow kinetics of some CB1 tracers has been acknowledged and discussed in the context of the challenges that arise in terms of required scan duration and quantification of PET data.[29] In this regard, the moderate affinity and faster kinetics of [11C]OMAR may offer some technical and practical advantages.

Like the other CB1 PET radiotracers, the uptake of [11C]OMAR generally agrees well with the density and distribution of CB1 receptors reported in human postmortem samples[4,5] (see Supplementary Figure 1). Exceptions common to all of the tracers include lower imaging outcomes in some limbic structures and higher imaging outcomes in the lentiform nucleus. In addition to methodological considerations such as the finite resolution of the PET imaging system, other investigators have commented on possible contributing factors including multiple *in vivo* affinity states of the receptor and its localization within the cell or its surface as part of a functional receptor reserve or active trafficking between the membrane and intracellular compartments.[10,13,24] Although the exact causes underlying these regionally specific discrepancies remain uncertain, the consistency across different PET radiotracers suggests that the phenomenon is real and warrants further study.

In our retest studies, the reproducibility of [11C]OMAR V_T expressed as mean absolute deviation was 7% to 10% (Table 1), which compares favorably to other CB1 tracers. For example, the mean absolute deviation for [18F]MK-9470 was 15% to 35%,[10,28] 10% to 20% for [11C]MePPEP,[8] and 9% to 17% for [18F]FMPEP-d_2.[9] It should be noted, however, that [11C]OMAR has lower V_T values and that its lower affinity leads to a reduced fraction of specific binding, so it is unclear whether the improved V_T reproducibility confers a genuine advantage. The superior intraclass correlation coefficient of [18F]FMPEP-d_2 over [11C]OMAR (~0.9 versus ~0.7) suggests that [18F]FMPEP-d_2 may offer better overall performance when assessing group differences. However, it is noteworthy that our study used the HRRT scanner with a reconstruction that includes line-spread function modeling whereas the test–retest studies with other tracers used the lower resolution Siemens ECAT HR+ or GE Advance camera with standard reconstruction and resolution-degrading filtering. These hardware and reconstruction differences are likely to result in higher resolution and better quantitation in our study, though perhaps at the expense of increased variance in the image data. The faster kinetics of [11C]OMAR also have the potential to permit shorter scans. In contrast to other CB1 tracers requiring at least 90 minutes of dynamic data and preferably 120 minutes or more, [11C]OMAR scans analyzed with MA1 showed no systematic bias for scans as short as 60 minutes, although it should be noted that analyses with $2T_V$ had more frequent convergence problems in a subset of regions for scans shorter than 90 minutes and that the variability of both MA1 and $2T_V$ estimates increased as scan duration was reduced. The ability to perform shorter scans would have practical implications in terms of patient scheduling and compliance. Although the short physical half-life of the 11C-radiolabel carries the usual limitations including the need for a cyclotron and radiochemistry facility on site, it also permits multiple scans in the same day and obviates the issue of defluorination and subsequent skull uptake, which has been reported as a confound for cortical uptake with [18F]FMPEP-d_2.[9]

In addition to potential contamination of cortex signal by radioactivity accumulating in the bone, estimates of V_T from [18F]FMPEP-d_2 data sets were found to increase gradually for scans longer than 120 minutes,[9] suggesting that radiometabolites may enter the brain despite the fact that the HPLC chromatogram showed all radiometabolites to be more polar than the parent. Interestingly, no uptick in V_T with increasing scan duration was observed with [11C]MePPEP,[8] even though both compounds are structurally quite similar and radiolabeled on the same moiety. For [11C]OMAR, radiometabolites were more polar than the parent in humans, a result that is consistent with those from mouse and baboon when [11C]OMAR was first characterized,[12] where it was reported that at least 94% of radioactivity in mouse brain was attributable to unchanged [11C]OMAR at 30 minutes after injection. Without the ability to directly assay radiometabolites in human brain, we sought to investigate empirically by conducting analyses of truncated data sets as was done for [11C]MePPEP and [18F]FMPEP-d_2. In most brain regions, V_T was found to be fairly insensitive to scan duration. With MA1 applied to 90 minutes of data, all 17 brain regions had V_T values within 5% of the terminal values obtained from the full 120-minute data set. Truncating further to 75 minutes, V_T values for all regions remained within 5% of their terminal values except for the central white matter, which was 7.7% lower. For 60-minute data sets, V_T values were reduced in the central white matter (−13.4%), cerebellar white matter (−12.2%), cerebellar cortex (−5.9%), and the occipital cortex (−5.7%). For all other regions, the differences were within 5% but there was an overall trend toward lower V_T with an average reduction of 3.3% ± 1.8%. Results from $2T_V$ analyses were similar but exhibited less sensitivity to scan duration (e.g., for the 60-minute data set, occipital cortex was 3.5% below the terminal value for $2T_V$ whereas MA1 had a negative bias of 5.7%). Based on these analyses, we cannot completely exclude the possibility of radiometabolites entering the brain; however, if they do, their effect is small in most regions.

In the present study, we observed significant differences between men and women in the radiometabolite fraction in the plasma (Figure 7B), net brain uptake as reflected by SUV (Figure 7E), and brain uptake relative to plasma as measured by V_T (Figure 7F). Differences in brain concentrations were not attributable to corresponding differences in gross bioavailability, as plasma protein binding did not differ between sexes (Figure 7A), although these very low f_P values are not likely to be highly reliable. Importantly, whereas SUV was greater in men, V_T was greater in women, since it includes the correction for the reduced plasma parent fraction in women. These findings are generally consistent with those from a previous study using [18F]MK-9470,[24] where greater plasma parent fraction and brain SUV were found in men. However, in that study no significant gender differences in the metabolite-corrected input function were observed in the initial cohort that underwent arterial blood sampling, so SUV was used as the final outcome measure. In contrast, we performed a full kinetic analysis of [11C]OMAR data using metabolite-corrected arterial input functions and V_T as the primary outcome parameter, with results opposite of the conclusions that would be drawn from SUV alone. Thus, our measurements conform with those previously reported for [18F]MK-9470 data, however, our interpretations disagree owing to the use of kinetic modeling methods and associated end points. Regarding the consistency of the gender effects reported here, we note that similar results have also been observed in a larger cohort of healthy subjects and in a patient population, as reported recently.[27] Whereas Van Laere *et al* reported age-dependent increases in radiotracer binding in women (but not in men) using an alternative CB1 radiotracer and different quantification techniques, we did not observe any significant age effects in [11C]OMAR binding in the brain regions that were analyzed. We note, however, that our findings should not be considered a confirmatory negative result because of two important limitations. First, the range of ages in our cohort was narrow, with most subjects in their 20's or early 30's, and only one man at 45 years of age. Second, the limited number of subjects in our study, while sufficient to draw sound conclusions about gender differences and kinetics of the radiotracer, do not provide the statistical power necessary for a definitive negative conclusion on age effect.

Our observation of significant sex differences in radiotracer metabolism and binding is an important finding, both in terms of the design and interpretation of studies and for understanding the role of the CB1 receptor in other sex-dependent differences.[30] Many studies using CB1 PET tracers have been conducted in cohorts consisting largely or exclusively of one sex or the other.[13,26,28,31–33] Several other studies had mixed-sex populations but did not explicitly note any significant sex effect.[34–36] In the two studies that reported sex dependence, one did not control for menstrual cycle

in women but noted no effect of current contraceptive use,[24] whereas the other—like the present study—imaged women during the follicular phase.[27] Although our present study and that of Van Laere *et al* both found elevated circulating tracer parent fraction and total brain uptake in men, opposite conclusions were drawn about the brain PET data because of differences in image analysis methods as described above. The discrepancy is not readily resolved by turning to the preclinical literature as studies in rodents using imaging and *in vitro* methods report elevated CB1 expression in male animals,[37] but results are frequently conflicting.[38] Moreover, such studies often did not account for the estrous cycle, but those that did typically show alterations attributable to menstrual phase and hormonal regulation.[37,39,40] The inconsistency in available data call for continued systematic study to investigate the interaction between the endocannabinoid receptor system and neurohormonal changes in both preclinical animals and clinical populations.

In this PET study with [11C]OMAR in humans, we found that the uptake and retention of the radiotracer in the brain were in strong concordance with alternative CB1 radiotracers and generally in good agreement with the density and distribution of CB1 receptors known from postmortem studies. Compartmental and graphical analyses were evaluated and it was determined that the 2T model inclusive of vascular correction was the preferred compartmental approach, and MA1 with $t^* = 30$ minutes performed best among the graphical techniques. These kinetic analysis results showed that V_T could be estimated with very good test–retest reproducibility, low intersubject variation, and no effect of scan order. As was reported previously for [18F]MK-9470, tracer parent fraction in plasma and tracer uptake in the brain differed between sexes in [11C]OMAR experiments. Although tracer uptake in the brain (as measured by SUV) was greater in men than women, V_T was greater in women than men. These results suggest that quantitative kinetic modeling with arterial input functions may lead to different interpretation of data than assessment of tracer uptake alone. From these findings, we recommend the use of MA1 method with metabolite-corrected arterial input functions and sex-matched control subjects when [11C]OMAR is used to study the CB1 receptor in patient populations.

CONCLUSION

In this PET imaging study in humans, we performed a comprehensive characterization of the CB1 PET radiotracer [11C]OMAR in a test–retest paradigm. Various kinetic analysis methods were assessed, and the 2T compartment model and MA1 method were found to provide reliable V_T estimates. Regional V_T displayed no systematic effect of scan order and very good test–retest reliability. In addition, we found significant sex differences in the behavior of the radiotracer: women had lower net brain uptake, but greater plasma metabolite fraction and higher regional V_T values. Taken together, data presented herein indicate that [11C]OMAR can be used to image the CB1 receptor in humans and reliably quantify regional binding parameters in the brain. However, sex differences in radiotracer metabolism and tissue binding should be taken into account when [11C]OMAR is used to measure CB1 receptor availability in patient populations.

DISCLOSURE/CONFLICT OF INTEREST

The authors declare no conflict of interest.

REFERENCES

1 Devane WA, Dysarz FA 3rd, Johnson MR, Melvin LS, Howlett AC. Determination and characterization of a cannabinoid receptor in rat brain. *Mol Pharmacol* 1988; **34**: 605–613.
2 Matsuda LA, Lolait SJ, Brownstein MJ, Young AC, Bonner TI. Structure of a cannabinoid receptor and functional expression of the cloned cDNA. *Nature* 1990; **346**: 561–564.
3 Munro S, Thomas KL, Abu-Shaar M. Molecular characterization of a peripheral receptor for cannabinoids. *Nature* 1993; **365**: 61–65.
4 Herkenham M, Lynn AB, Little MD, Johnson MR, Melvin LS, de Costa BR *et al.* Cannabinoid receptor localization in brain. *Proc Natl Acad Sci USA* 1990; **87**: 1932–1936.
5 Glass M, Dragunow M, Faull RL. Cannabinoid receptors in the human brain: a detailed anatomical and quantitative autoradiographic study in the fetal, neonatal and adult human brain. *Neuroscience* 1997; **77**: 299–318.
6 Mechoulam R, Parker LA. The endocannabinoid system and the brain. *Annu Rev Psychol* 2013; **64**: 21–47.
7 Horti AG, Van Laere K. Development of radioligands for in vivo imaging of type 1 cannabinoid receptors (CB1) in human brain. *Curr Pharm Des* 2008; **14**: 3363–3383.
8 Terry GE, Liow JS, Zoghbi SS, Hirvonen J, Farris AG, Lerner A *et al.* Quantitation of cannabinoid CB1 receptors in healthy human brain using positron emission tomography and an inverse agonist radioligand. *Neuroimage* 2009; **48**: 362–370.
9 Terry GE, Hirvonen J, Liow JS, Zoghbi SS, Gladding R, Tauscher JT *et al.* Imaging and quantitation of cannabinoid CB1 receptors in human and monkey brains using [18F]-labeled inverse agonist radioligands. *J Nucl Med* 2010; **51**: 112–120.
10 Burns HD, Van Laere K, Sanabria-Bohorquez S, Hamill TG, Bormans G, Eng WS *et al.* [18F]MK-9470, a positron emission tomography (PET) tracer for in vivo human PET brain imaging of the cannabinoid-1 receptor. *Proc Natl Acad Sci USA* 2007; **104**: 9800–9805.
11 Tsujikawa T, Zoghbi SS, Hong J, Donohue SR, Jenko KJ, Gladding RL *et al.* In vitro and in vivo evaluation of 11C-SD5024, a novel PET radioligand for human brain imaging of cannabinoid CB1 receptors. *Neuroimage* 2014; **84**: 733–741.
12 Horti AG, Fan H, Kuwabara H, Hilton J, Ravert HT, Holt DP *et al.* 11C-JHU75528: a radiotracer for PET imaging of CB1 cannabinoid receptors. *J Nucl Med* 2006; **47**: 1689–1696.
13 Wong DF, Kuwabara H, Horti AG, Raymont V, Brasic J, Guevara M *et al.* Quantification of cerebral cannabinoid receptors subtype 1 (CB1) in healthy subjects and schizophrenia by the novel PET radioligand [11C]OMAR. *Neuroimage* 2010; **52**: 1505–1513.
14 Logan J, Fowler JS, Volkow ND, Wolf AP, Dewey SL, Schlyer DJ *et al.* Graphical analysis of reversible radioligand binding from time-activity measurements applied to [*N*-11C-methyl]-(-)-cocaine PET studies in human subjects. *J Cereb Blood Flow Metab* 1990; **10**: 740–747.
15 Carson RE, Barker WC, Liow JS, Johnson C. Design of a motion-compensation OSEM list-mode algorithm for resolution-recovery reconstruction for the HRRT. *IEEE Nucl Sci Symp Conf Rec* 2004; **5**: 3281–3285.
16 Hilton J, Yokoi F, Dannals RF, Ravert HT, Szabo Z, Wong DF. Column-switching HPLC for the analysis of plasma in PET imaging studies. *Nucl Med Biol* 2000; **27**: 627–630.
17 Jenkinson M, Bannister P, Brady M, Smith S. Improved optimization for the robust and accurate linear registration and motion correction of brain images. *Neuroimage* 2002; **17**: 825–841.
18 Papademetris X, Jackowski MP, Rajeevan N, DiStasio M, Okuda H, Constable RT *et al.* BioImage Suite: an integrated medical image analysis suite: an update. *Insight J* 2006; **2006**: 209.
19 Tzourio-Mazoyer N, Landeau B, Papathanassiou D, Crivello F, Etard O, Delcroix N *et al.* Automated anatomical labeling of activations in SPM using a macroscopic anatomical parcellation of the MNI MRI single-subject brain. *Neuroimage* 2002; **15**: 273–289.
20 Innis RB, Cunningham VJ, Delforge J, Fujita M, Gjedde A, Gunn RN *et al.* Consensus nomenclature for in vivo imaging of reversibly binding radioligands. *J Cereb Blood Flow Metab* 2007; **27**: 1533–1539.
21 Ichise M, Toyama H, Innis RB, Carson RE. Strategies to improve neuroreceptor parameter estimation by linear regression analysis. *J Cereb Blood Flow Metab* 2002; **22**: 1271–1281.
22 Akaike H. A new look at the statistical model identification. *IEEE Trans Automatic Control* 1974; **19**: 716–723.
23 Schwarz G. Estimating the dimension of a model. *Ann Stat* 1978; **6**: 461–464.
24 Van Laere K, Goffin K, Casteels C, Dupont P, Mortelmans L, de Hoon J *et al.* Gender-dependent increases with healthy aging of the human cerebral cannabinoid-type 1 receptor binding using [18F]MK-9470 PET. *Neuroimage* 2008; **39**: 1533–1541.
25 Slifstein M, Laruelle M. Effects of statistical noise on graphic analysis of PET neuroreceptor studies. *J Nucl Med* 2000; **41**: 2083–2088.
26 Neumeister A, Normandin MD, Murrough JW, Henry S, Bailey CR, Luckenbaugh DA *et al.* Positron emission tomography shows elevated cannabinoid CB1 receptor binding in men with alcohol dependence. *Alcohol Clin Exp Res* 2012; **36**: 2104–2109.
27 Neumeister A, Normandin MD, Pietrzak RH, Piomelli D, Zheng MQ, Gujarro-Anton A *et al.* Elevated brain cannabinoid CB1 receptor availability in post-traumatic stress disorder: a positron emission tomography study. *Mol Psychiatry* 2013; **18**: 1034–1040.

28 Sanabria-Bohorquez SM, Hamill TG, Goffin K, De Lepeleire I, Bormans G, Burns HD *et al.* Kinetic analysis of the cannabinoid-1 receptor PET tracer [18F]MK-9470 in human brain. *Eur J Nucl Med Mol Imaging* 2010; **37**: 920–933.
29 Hirvonen J, Terry GE, Halldin C, Pike VW, Innis RB. Approaches to quantify radioligands that wash out slowly from target organs. *Eur J Nucl Med Mol Imaging* 2010; **37**: 917–919.
30 Fattore L, Fratta W. How important are sex differences in cannabinoid action? *Br J Pharmacol* 2010; **160**: 544–548.
31 Van der Schueren BJ, Van Laere K, Gerard N, Bormans G, De Hoon JN. Interictal type 1 cannabinoid receptor binding is increased in female migraine patients. *Headache* 2012; **52**: 433–440.
32 Hirvonen J, Zanotti-Fregonara P, Umhau JC, George DT, Rallis-Frutos D, Lyoo CH *et al.* Reduced cannabinoid CB1 receptor binding in alcohol dependence measured with positron emission tomography. *Mol Psychiatry* 2013; **18**: 916–921.
33 Gerard N, Pieters G, Goffin K, Bormans G, Van Laere K. Brain type 1 cannabinoid receptor availability in patients with anorexia and bulimia nervosa. *Biol Psychiatry* 2011; **70**: 777–784.
34 Ceccarini J, De Hert M, Van Winkel R, Peuskens J, Bormans G, Kranaster L *et al.* Increased ventral striatal CB1 receptor binding is related to negative symptoms in drug-free patients with schizophrenia. *Neuroimage* 2013; **79**: 304–312.
35 Van Laere K, Casteels C, Lunskens S, Goffin K, Grachev ID, Bormans G *et al.* Regional changes in type 1 cannabinoid receptor availability in Parkinson's disease in vivo. *Neurobiol Aging* 2012; **33**: 620. e1-e8.
36 Van Laere K, Goffin K, Bormans G, Casteels C, Mortelmans L, de Hoon J *et al.* Relationship of type 1 cannabinoid receptor availability in the human brain to novelty-seeking temperament. *Arch Gen Psychiatry* 2009; **66**: 196–204.
37 Riebe CJ, Hill MN, Lee TT, Hillard CJ, Gorzalka BB. Estrogenic regulation of limbic cannabinoid receptor binding. *Psychoneuroendocrinology* 2010; **35**: 1265–1269.
38 Casteels C, Gerard N, van Kuyck K, Pottel L, Nuttin B, Bormans G *et al.* Small animal PET imaging of the type 1 cannabinoid receptor in a rodent model for anorexia nervosa. *Eur J Nucl Med Mol Imaging* 2014; **41**: 308–321.
39 Castelli MP, Fadda P, Casu A, Spano MS, Casti A, Fratta W *et al.* Male and female rats differ in brain cannabinoid CB1 receptor density and function and in behavioural traits predisposing to drug addiction: effect of ovarian hormones. *Curr Pharm Des* 2014; **20**: 2100–2113.
40 Rodriguez de Fonseca F, Cebeira M, Ramos JA, Martin M, Fernandez-Ruiz JJ. Cannabinoid receptors in rat brain areas: sexual differences, fluctuations during estrous cycle and changes after gonadectomy and sex steroid replacement. *Life Sci* 1994; **54**: 159–170.

Supplementary Information accompanies the paper on the Journal of Cerebral Blood Flow & Metabolism website (http://www.nature.com/jcbfm)